Morphological Evolution of Poly(ethylene terephthalate) during Equal Channel Angular Extrusion Process

Z.-Y. Xia and H.-J. Sue*

Polymer Technology Center, Department of Mechanical Engineering, Texas A&M University, College Station, Texas 77843-3123

T. P. Rieker

Center for Microengineered Materials, Department of Chemical and Nuclear Engineering, University of New Mexico, Albuquerque, New Mexico 87131

Received June 29, 2000; Revised Manuscript Received September 21, 2000

ABSTRACT: Highly textured semicrystalline poly(ethylene terephthalate) (PET) prepared through an equal channel angular extrusion (ECAE) process was studied using small-angle X-ray scattering (SAXS), transmission electron microscopy (TEM), optical microscopy (OM), differential scanning calorimetry (DSC), and annealing tests. OM results indicate that the original spherulites are highly elongated after ECAE. SAXS and TEM results indicate that, after one ECAE pass, two types of lamellar orientations are induced: one with the lamellar normal perpendicular to the flow direction and the other tilted at an angle of approximately 45° counterclockwise away from the flow direction. Annealing tests suggest that interlamellar compression is the dominant mechanism for the deformation of the amorphous phase.

Introduction

Controlled morphology and anisotropy are highly desired for improving the physical and mechanical properties of polymeric materials. It has been documented that high modulus, high fracture toughness, good weatherability, and improved solvent resistance can be achieved through controlled morphology.[1−3] Since the 1960s, many research and experimental efforts have been dedicated to achieving controlled morphology in polymers, especially in semicrystalline polymers.[4−13]

It is believed that, during the deformation of semicrystalline polymers, the amorphous phase will deform first.[4,5] The proposed deformation mechanisms for the amorphous phase include interlamellar shear, interlamellar separation/compression, and lamellar stack rotation.[5] Keller and Hay[6] first reported the existence of interlamellar shear and interlamellar separation mechanisms in the study of polyethylene (PE). These two mechanisms are favored if the amorphous phase between lamellae is soft and easy to deform, especially at temperatures higher than the glass transition temperature (T_g) of the amorphous phase. Lamellar stack rotation happens along with interlamellar shear and interlamellar separation and is not considered as an independent mechanism.[7]

When the deformation of the amorphous phase is consumed, i.e., the amorphous phase is fully strained, the deformation of the crystalline phase will take place. Three different modes have been documented to accommodate the deformation of the crystalline phase. They are crystallographic slip, mechanical twinning, and martensitic transformation.[8] Crystallographic slip is the most important deformation mode for the crystalline phase. It happens either parallel to the molecular chain direction, i.e., chain slip, or normal to the molecular chain direction, i.e., transverse slip. Chain slip can be activated more easily since it has a smaller Burgers vector.[5,8] Evidence of slip in several semicrystalline polymers has been reported.[4−6,9,10] The recent modeling study[11−13] also suggests that crystallographic slip is the main deformation mode for the crystalline phase. Mechanical twinning and martensitic transformation do not contribute much to the plastic deformation of semicrystalline polymers.[4] However, they help bring the crystals into favorable positions for crystallographic slip to occur.

The above findings are obtained primarily based on PE. Poly(ethylene terephthalate) (PET) has many important applications where controlled morphology is greatly appreciated. Most of the deformation and orientation studies on PET are on amorphous PET.[14−17] Strain-induced crystallization (SIC) has been found to be an important orientation phenomenon in amorphous PET.[14−16] Compared to the amorphous PET system, research on semicrystalline PET is quite limited. Göschel et al.[18] found that the *c*-axis of the PET crystal is aligned along the drawing direction after being fully stretched. The work by Bellare et al.[10] showed that, during plane strain compression of PET, the original spherulites are transformed into fragmented lamellae with the lamellar normals parallel to the flow direction. The (100)[001] chain slip is the first observed mechanism and operates throughout the deformation. At a later stage of deformation, (010)[001] transverse slip occurs. A mesomorphic phase with neumatic order has also been observed by several researchers[19−21] during the orientation of semicrystalline PET.

The methods for orienting polymers in the above studies include tensile stretching,[22] uniaxial compression,[23] plane strain compression,[9] and rolling.[24,25] As a nearly "ideal" deformation mode for creating structure and texture of interest, simple shear has been shown to be an important material processing technique for metallic materials.[26−29] Unfortunately, little attention has been given to the simple shear deformation of polymeric materials.[4,30,31]

* Corresponding author. E-mail hjsu@acs.tamu.edu; phone (979) 845-5024.

10.1021/ma001140w CCC: $19.00
Published on Web 10/25/2000

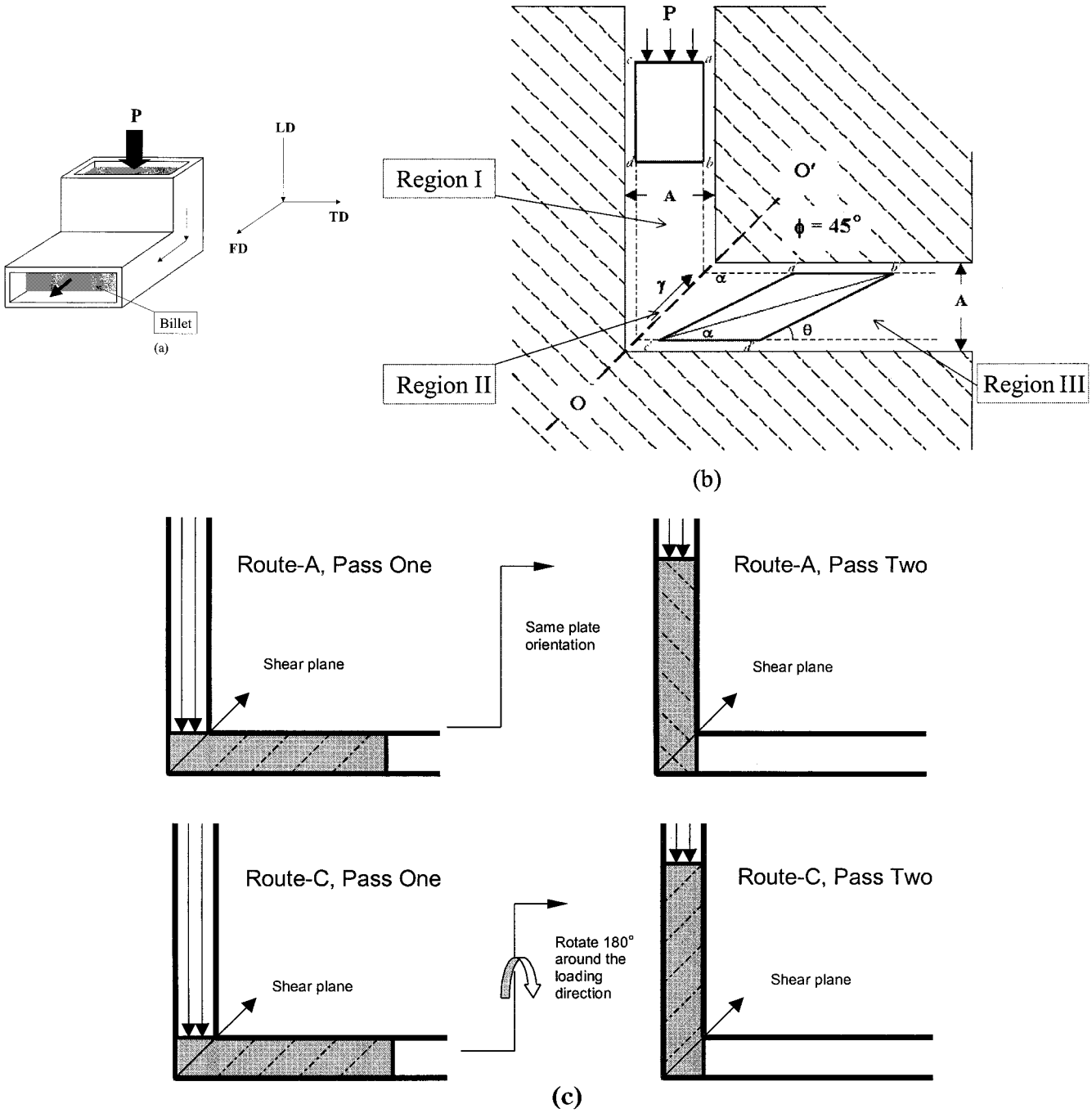

Figure 1. (a) ECAE die fixture. LD = loading direction, TD = transverse direction, and FD = flow direction. (b) Schematic of ECAE die showing the deformation of the billet. The transitional line OO′ is the shear direction. Regions I, II, and III are defined as stressed but before passing through the die angular region, in the die angular region, and after passing through the die angular region, respectively. (c) Schematic of route A and route C ECAE processes.

The goal of this research is to use the simple shear concept to probe the lamellar scale morphology evolution of semicrystalline PET subjected to simple shear conditions. The equal channel angular extrusion (ECAE) process is chosen for this purpose. Owing to the nature of the ECAE, a high level of simple shear deformation can be achieved in the billet. Compared with conventional polymer processing methods, such as drawing, hydrostatic extrusion, and rolling, the ECAE technique offers several significant advantages.[32−34] First, ECAE can induce controlled molecular orientation in bulk polymers without changing the geometry of the specimen. Hence, the extrusion can be repeated multiple times until the desired properties are achieved in the extrudate. Second, the ECAE process can generate different modes of controlled molecular orientation in the extrudate by changing the extrudate orientation at subsequent ECAE passes.[26,35,36] If the extrudate is processed along the same orientation at each pass, called route A, a progressively increased shear strain ($\gamma = 2N \cot \phi$) will be experienced by the extrudate (Figure 1). If the extrusion is performed by rotating the specimen by 180° around its loading axis after the previous pass, called route C, then the global simple shear strain experienced by the specimen will, in theory, be removed. However, the local scale molecular orientation will still be preserved.

In this research, semicrystalline PET processed by route A, one pass (A1) ECAE process is investigated. The corresponding structural evolution process during

ECAE is reported. The usefulness of ECAE for studying the deformation behavior of polymers is also discussed. Morphological evolution of PET subjected to multiple ECAE passes will be reported in a subsequent paper.

Experimental Section

Sample Preparation and the ECAE Process. PET (ENSITEP) sheets with a nominal thickness of 9.525 mm were obtained from Insinger Inc. The sheets were then machined into dimensions of 152.40 mm × 152.40 mm × 9.525 mm to fit the die for ECAE process. Grid lines, with 2.0 mm × 2.0 mm square in size, were milled on the two side surfaces of PET sample before extrusion to experimentally quantify the shear strain in the extrudate after ECAE.

A J-type thermocouple (Omega GA5TC-GG-J-24-36) was embedded in the PET billet to monitor the billet temperature during the extrusion. Plunger traveling distance, applied load, and temperature were recorded during the extrusion. A servo-hydraulic driven mechanical testing system (MTS-810) was employed for the extrusion using the die fixture shown in Figure 1a. An antiseize lubricant (Permatex Industrial-80208) was used to minimize the friction between the billet and the die inner surfaces. The extrusions were performed at room temperature with extrusion rates ranging from 0.014 to 0.51 mm/s.

For clarity, the extrusion process is divided into three regions for discussion (Figure 1b): region I, material is compressed but before passing through the right angle of the die; region II, material is in the die right angle area; region III, material is in the extruded region. Furthermore, three directions that describe the ECAE process are defined in this paper: flow direction (FD), loading direction (LD), transverse direction (TD), as shown in Figure 1a.

All samples for testing and characterization were carefully prepared in a consistent manner to ensure that the structural changes in the PET extrudate are due to the ECAE process alone. Samples before and after ECAE were cut from similar locations of the billet. They were then polished to the desired thickness. All samples were continuously cooled with water to avoid any annealing effect due to cutting or polishing.

Optical Microscopy. Optical microscopy (OM), Olympus model BX60, under cross-polarized field was used to observe the spherulitical structure changes. Samples were polished to about 25 μm in thickness prior to OM observations.

Small-Angle X-ray Scattering. Small-angle X-ray scattering (SAXS) measurements were performed at the University of New Mexico/Sandia National Laboratories Small-angle X-ray Scattering Lab using the 5 m pinhole instrument.[37]

Samples with dimensions of 8 mm × 8 mm × 0.2 mm were cut from various locations on a partially extruded PET block and then polished to the desired thickness. All the samples were marked to determine the preferred long period orientations with respect to FD. The samples were oriented in the SAXS instrument with the incident beam perpendicular to the plane of the sample. In this geometry, the 2-D detector image directly shows anisotropy distribution of lamellae (via the long period) in the plane of the sample.

Plots showing preferred orientation, i.e., intensity vs azimuthal angle (I vs χ), are produced from the 2-D SAXS images by integrating over the scattering angle 2θ. We refer to a preferred orientation direction as a domain. These domains are collections of lamellae with a wide mosaic in both the long period and its orientation. The latter leads to a two-lobed scattering pattern in the 2-D SAXS images for a single preferred orientation domain.

Intensity vs scattering angle (I vs 2θ) data are obtained by integrating the 2-D SAXS images over a range of azimuthal angle χ. Plots of I vs 2θ show broad peaks attributed to the long period.

Since there remains a significant disorder in the long period, i.e., disorder in lamellar orientation, even in samples that demonstrate preferred orientation, the ECAE processed PET is only partially oriented. According to the work of Ruland,[38] Lorentz corrected intensity (q^2I) is needed for such systems,[38−40]

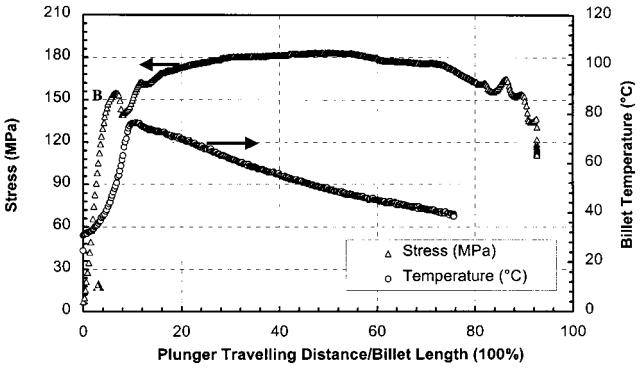

Figure 2. Load (stress) and temperature versus plunger traveling distance normalized by the billet length for PET extruded at room temperature and at an extrusion rate of 0.51 mm/s.

where $q = 4\pi/\lambda \sin\theta$ and $\lambda = 0.154$ nm. The Lorentz correction can be used for both isotropic and partially oriented polymers.[38] The long period is determined from the Lorenz plots (q^2I vs q) of the background corrected scattering data.

Transmission Electron Microscopy. The transmission electron microscopy (TEM) observations were conducted using a Zeiss-10C microscope operating at an accelerated voltage of 100 kV. Samples with a cross-sectional area of 2 mm × 2 mm were carefully prepared from a location similar to that of the samples prepared for SAXS analyses. The samples were then trimmed into a pyramid shape with the size of the surface of interest being 0.3 mm × 0.3 mm. A glass knife was used to face off the trimmed block. The faced-off sample was stained with ruthenium tetraoxide (RuO_4) vapor for 10 h at 25 °C. The stained surface was then ultrathinsectioned into a thickness of 80 nm with a diamond knife using a Reichert Ultracut-E ultramicrotome. The thin sections were collected with a 100 mesh Formvar copper grid.

Annealing Test. The annealing test was carried out at temperatures ranging from 50 to 214 °C to investigate the deformation recovery of the amorphous phase. Samples with 8 mm × 8 mm × 2 mm in size were chosen for the tests. The thickness of 2 mm was found to give a flat surface after annealing; i.e., the sample did not warp. The low-temperature (<180 °C) annealing tests were conducted in a heated silicon oil bath. The high-temperature (>200 °C) annealing tests were performed in an oven. The samples were immersed in a silicon oil bath/or in an oven for 2 min. Afterward, the dimensional changes of the sample were recorded. The temperature was controlled at ±1 °C during the annealing tests.

Density Measurements. Density measurements were performed via the displacement method as described in ASTM-D792. Sample weights in air and in 2-propanol (0.785 g/cm^3) were measured.

Heat of Fusion. A differential scanning calorimeter (DSC) (Perkin-Elmer Pyris-1) was employed to scan the sample over the temperature range 25−300 °C at a heating rate of 10 °C/min. Temperature integration ranges from 100 to 280 °C were used for the heat of fusion measurement.[41] The sample weight for DSC measurements was about 10 mg.

Results

Solid-State Deformation Process. Figure 2 shows the typical loading stress and billet temperature vs plunger traveling distance profile during ECAE.

In the early stage of the extrusion, i.e., under a small strain level, the deformation is primarily elastic. The material conforms to the die channel cavity. At this stage (from point A to point B in Figure 2), the deformation mainly comes from the soft amorphous phase. This deformation is mostly recoverable upon unloading.[4,8]

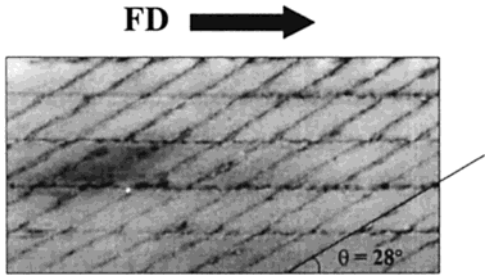

Figure 3. Grid-line change after A1 ECAE process. The extrusion was performed at room temperature and at an extrusion rate of 0.51 mm/s.

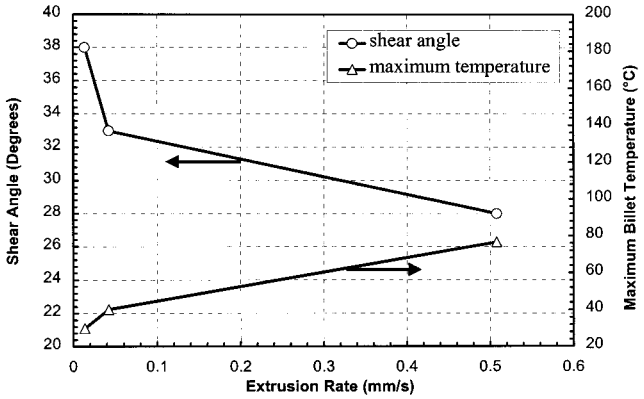

Figure 4. Extrusion rate effect on shear angle (θ) and billet temperature for A1 ECAE process.

Upon reaching point B, the material begins to yield, and plastic deformation begins to take place. As the extrusion proceeds further, the deformation of amorphous phase is consumed, and the deformation of the crystalline phase ensues.

Figure 3 shows that the original square grid lines are deformed and tilted at an angle (θ) away from FD. The ECAE induced shear strain (γ) is defined as cot (θ). For extrusions performed at an extrusion rate of 0.51 mm/s and under room temperature, the tilt angle (θ) is 28°. This equals to an induced shear strain of 190% (cot 28°). On the basis of the pattern of the deformed grid lines, it is evident that the shear deformation is uniform across the thickness direction of the billet (Figure 3). A temperature rise of 50 °C was observed in the billet during A1 ECAE process (Figure 2). Both the induced shear strain and temperature rise are found to increase with increasing extrusion rates (Figure 4).

Sample A1 processed at room temperature and at an extrusion rate of 0.51 mm/s is used for structural characterization since the maximum shear strain is observed in the extrudates under this extrusion condition for the present study.

Deformation of the Crystalline Phase. 1. Spherulitical Scale. Figure 5 shows the cross-polarized optical micrographs of the thin sections prepared before and after ECAE. All the samples were cut along the LD-FD plane. It appears that the original spherulites are highly elongated into ellipsoids after A1 ECAE (Figure 5b). Further analyses of Figure 5b indicate that the long axis of the ellipsoid is at an angle (α) of about 24° counterclockwise away from FD.

2. Lamellar Scale. Figure 6a shows the as-collected 2-D SAXS patterns for reference and A1 ECAE-processed PET samples. The samples **1b**, **2b**, **3b**, **1a**, **3a**, and **5a** were cut along the three orthogonal directions: LD, TD, and FD before (**b** samples) and after (**a** samples) extrusion. Samples **2b** and **3a** were cut in the center of the billet and then polished to the desired thickness. Specimen **4a** was cut at an angle of 45° counterclockwise away from FD, while specimen **2a** was cut perpendicular to **4a**. All the above samples are mounted on the SAXS sample wheel with the sample reference direction intercepts the detector at $\chi = 115°$ and $295 \pm 5°$. Since SAXS directly detects the long period orientation, i.e., the lamellar normal orientation, the lamellar normal is used to describe the lamellar orientation throughout this paper.

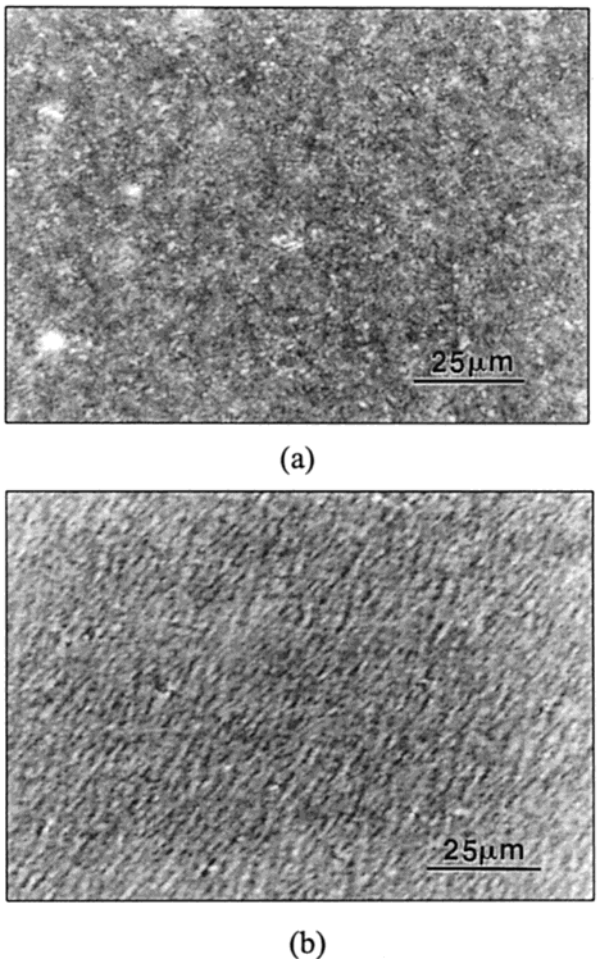

Figure 5. Cross-polarized OM micrographs of PET: (a) before and (b) after A1 ECAE. FD is vertical in (b).

Table 1. SAXS Determined Long Periods

sample	domain	fwhh[a] (χ, deg)	peak position (q_{max}, nm^{-1})	long period ($2\pi/q_{max}$, nm)
1b	isotropic		0.58	10.8
2b	isotropic		0.69	9.1
3b	isotropic		0.55	11.4
1a	α, β	45, 50	0.59, 0.71	10.6, 8.8
3a	isotropic		0.69	9.1
5a	β	55	0.74	8.5
2a	α	46	0.63	10.0
4a	isotropic		0.64	9.8
scan 9	α, β	60, 70	0.59, 0.62	10.6, 10.1
scan 5	α, β	60, 50	0.61, 0.73	10.3, 8.6

[a] fwhh: full width at half-height.

Figure 6b shows the Lorenz plot for sample **3b**, which has an isotropic distribution of lamellae. To determine the long period of isotropic sample, the entire 2-D image is integrated ($0 < \chi < 360°$) over the azimuthal angle. As shown in Figure 6b, q_{max} is 0.55 nm^{-1}for sample **3b**, which yields a long period of $d = 2\pi/q_{max} = 11.4$ nm.

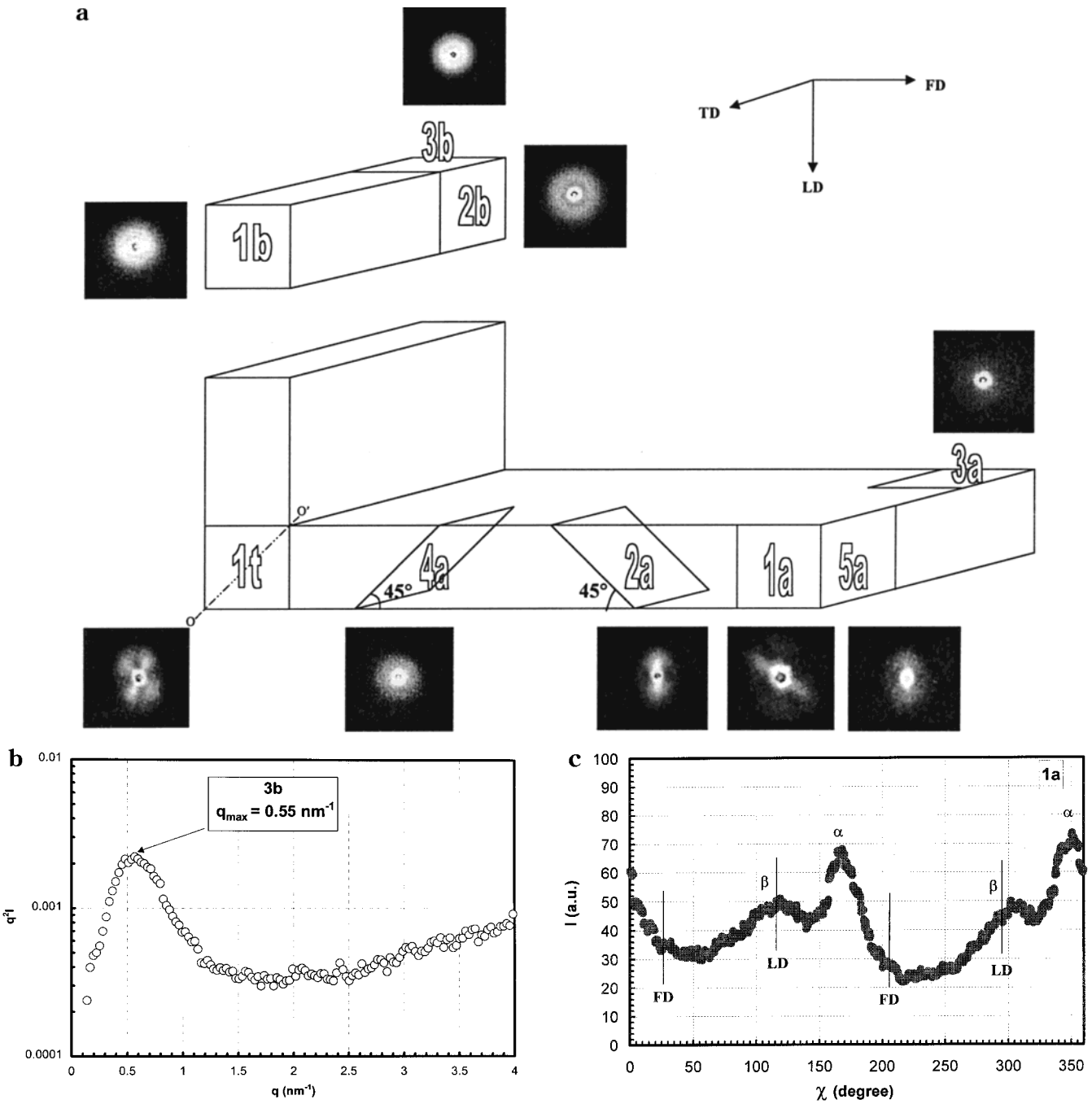

Figure 6. (a) 2-D SAXS patterns. (b) Lorentz plot of **3b**. The upturn in the high q range comes from the amorphous halo.[43] (c) I vs χ plot for sample **1a**.

For anisotropic 2-D images, a wedge shaped region spanning the full width at half-height (fwhh) of one of the preferred orientation lobes is integrated. The long period is determined in a consistent manner of all the samples investigated. The results are listed in Table 1.

The initial distribution of lamellae in the billet before extrusion is relatively isotropic as shown by the 2-D SAXS images for samples **1b**, **2b**, and **3b** in Figure 6a. The long periods for samples **1b**, **2b**, and **3b** are 10.8, 9.1, and 11.4 nm, respectively (Table 1). The isotropic distribution of lamellae in **1b** is confirmed by TEM investigation of several locations in this sample.

Five samples (**1a**, **2a**, **3a**, **4a**, and **5a**) were examined in order to ascertain the three-dimensional lamellar orientation in the fully extruded region (III). Sample **1a**, which is parallel to LD-FD plane, shows two domains of preferred lamellar orientation. As shown by the I vs χ plot for sample **1a** in Figure 6c, the first preferred lamellar orientation, labeled as α-lamellar domain, is oriented with the lamellar domain normal at an angle of 45° clockwise from FD. The second, labeled as β-lamellar domain normal, lies perpendicular to FD. The long periods of the α- and β-lamellar domains are 10.6 and 8.8 nm, respectively (Table 1). The angle between the α- and β-lamellar domains is 45°. The remaining samples show orthogonal views of these two lamellar domains: samples **2a** and **4a** for the α-lamellar domain and samples **3a** and **5a** for the β-lamellar domain. Both the α- and β-lamellar domains have orthorhombic symmetry.

To probe the lamellar evolution during ECAE, sample **1t**, which contains FD, LD, and the transition line OO′,

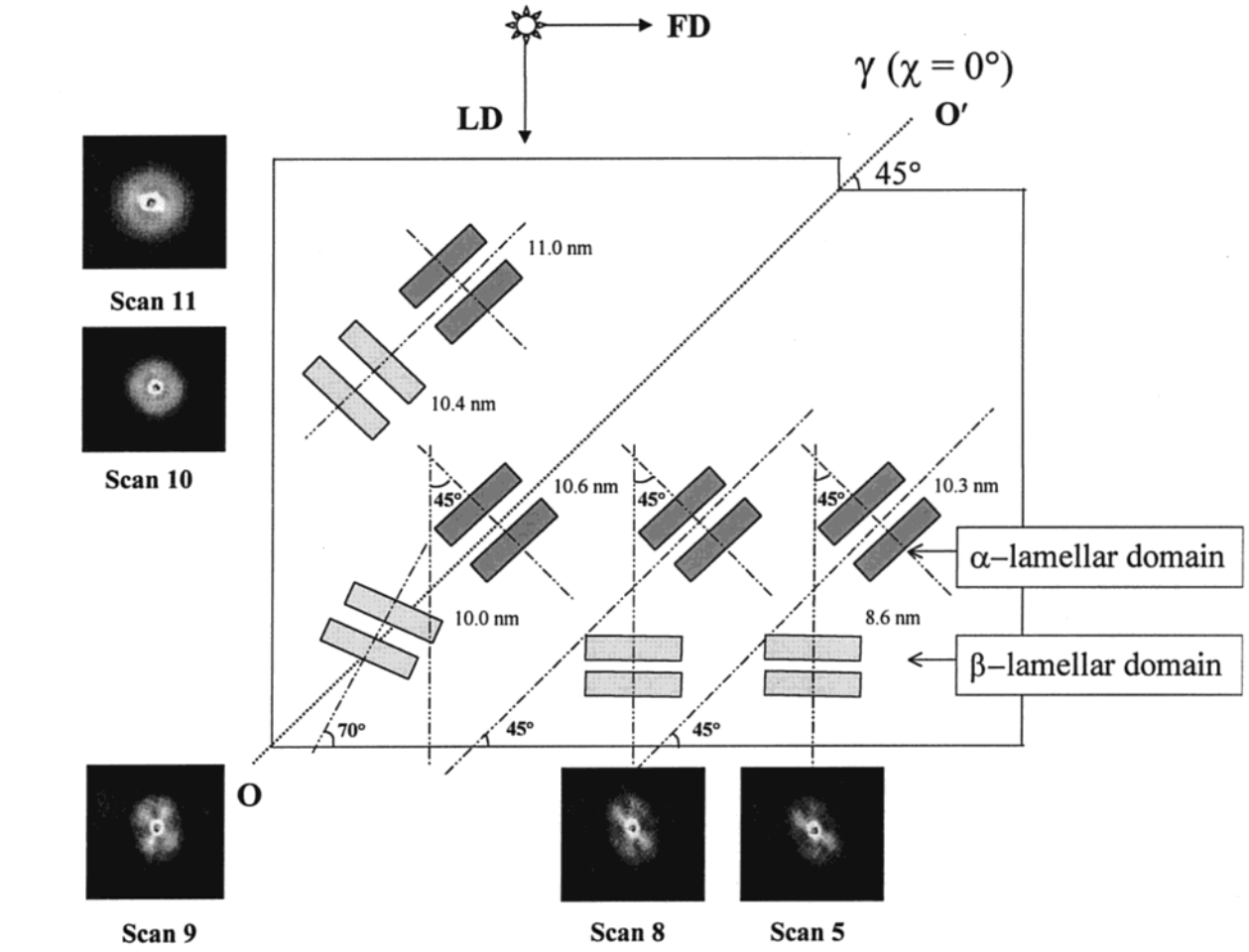

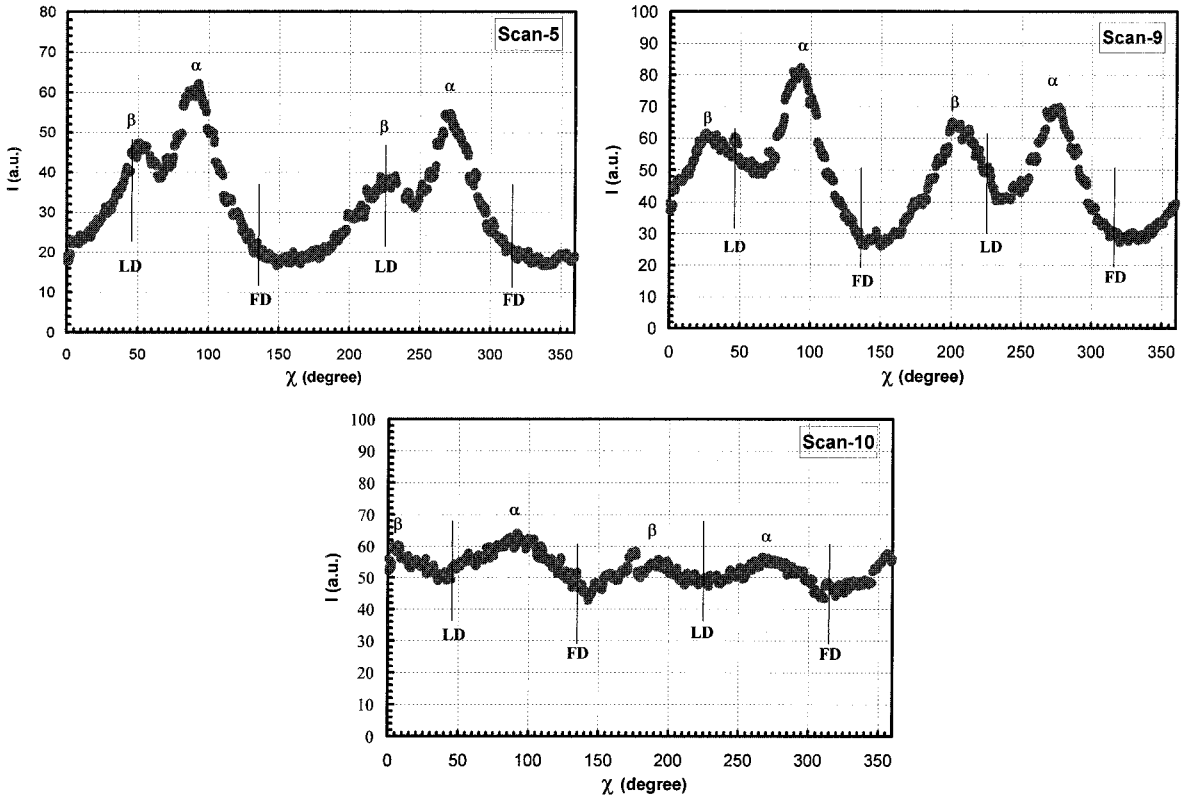

Figure 7. SAXS analyses of the transition zone sample **1t**: (a, upper) evolution of lamellar orientation; (b, lower) *I* vs χ plots for scans 5, 9, and 10.

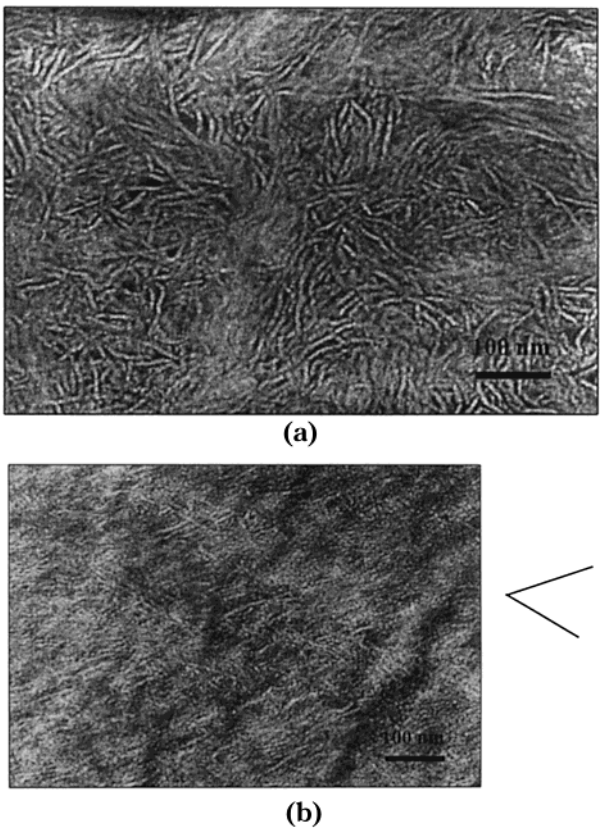

Figure 8. TEM micrographs showing the lamellar structure of PET: (a, top) before ECAE and (b, bottom) after A1 ECAE process. The "V-shape" next to (b) illustrates the lamellar orientation in sample A1. Both micrographs were taken along the transverse direction.

was cut from the die transitional zone (region II). This sample was mounted in the sample wheel with the transition line (OO′) vertical, crossing the detector at $\chi = 0°$ and $180 \pm 5°$. Fifteen scans were made across this specimen, in a line perpendicular to OO′ with an increment of 1 mm per scan starting in the extruded region (III). Figure 7a shows the 2-D SAXS patterns from selected scans. The evolution of preferred lamellar orientation is apparent. Scans 11−15 (only scan 11 is shown here) cover region (I) and show a relatively isotropic SAXS pattern. However, as the X-ray beam approaches the transition line OO′ (scan 10), two weakly preferred lamellar orientations become evident (Figure 7b). At the transition line OO′ (scan 9), two well-defined domains of preferred lamellar orientation are obtained. The analyses of the I vs χ plot of scan 9 (Figure 7b) reveals that the α-lamellar domain, with a long period of 10.6 nm, is oriented with the lamellar domain normal at an angle of approximately 45° counterclockwise away from LD. The normal of the β-lamellar domain tilts at an angle of approximately 70° counterclockwise from FD and has a long period of 10.1 nm. The orientation of the α-lamellar domain normal appears to stay at 45° in the subsequent scans moving away from the transition region (II) into the extruded region (III), as shown in Figure 7. The orientation of the β-lamellar domain normal, however, continues to rotate counterclockwise until it lies perpendicular to FD in the fully extruded region (scan 5 in Figure 7a).

To verify the SAXS results, TEM was performed. Figure 8 shows the TEM micrographs of the reference and A1 PET samples. The samples are cut parallel to the LD-FD plane before and after extrusion, respectively. Figure 8a shows that the lamellae are randomly oriented before ECAE. After the A1 ECAE process, a "V-type" of lamellar orientation with the angle of roughly 45° is observed (Figure 8b). Both of these findings are consistent with the SAXS results. Further, Figure 8b reveals that the lamellae in sample A1 have become thinner and more closely packed, which suggests the occurrence of lamellar thinning, interlamellar shear, and interlamellar compression. The observed lamellar thinning is confirmed by the SAXS correlation function analyses.[42] Lamellar thinning has also been found in the ECAE of semicrystalline linear low-density polyethylene (LLDPE) via the ECAE process.[32]

3. Deformation of the Amorphous Phase. Owing to the randomness of the amorphous phase, it is difficult to find a proper method to characterize the deformation of the amorphous phase in semicrystalline polymers. The annealing test, when performed between T_g and the melting point (T_m), has been shown to be a useful technique for probing deformation of the amorphous phase in semicrystalline polymers.[44] In this section, the annealing tests on the ECAE processed PET are performed to examine the ECAE-induced deformation in the amorphous phase.

In the ECAE-processed PET, if interlamellar shear or interlemellar separation are induced, then the annealing test at $T_g < T < T_m$ should relax the strained amorphous phase, and the original shape of the extrudate should be partially recovered. Figure 9 shows the annealing test results of ECAE-processed PET. Sample **1a**, which is cut parallel to the LD-FD plane from sample A1, does not show any appreciable change in shape when the annealing temperature (T_a) was below T_g (76 °C). When T_a is higher than T_g, the shape of the sample recovers toward its original shape owing to the relaxation of the amorphous phase. The extent of the shape recovery increases with T_a. However, as T_a approaches T_m, the shape recovery becomes less pronounced (Figure 9a). This is probably because some of the amorphous phase is "locked" in the newly formed crystalline structure. Complete shape recovery would need to break the crystalline structure, which requires T_a to be higher than T_m. Sample **5a**, which is cut perpendicular to the FD, only shows the changes in height and width (Figure 9b). This is consistent with the annealing effect from sample **1a**. To ascertain that the sample geometry changes during annealing are due to ECAE, a reference PET sample was also annealed under similar conditions. However, no appreciable changes in size and shape could be found even when annealed up to 200 °C. Consequently, we conclude that the geometry changes during annealing are due to the ECAE process.

By combining the annealing test results of **1a** and **5a**, it is evident that interlamellar shear and interlamellar compression (Figure 9b) are the dominant deformation mechanisms for the amorphous phase during the A1 ECAE process.

The DSC analyses shown in Table 2 indicate that the melting enthalpy (ΔH) for PET increases with extrusion, i.e., $\Delta H_{III} > \Delta H_I > \Delta H_{ref}$. The subscripts, III, I, and ref have the same meaning as in the SAXS section. The increase in ΔH may be due either to an increase in crystallinity through stress/strain-induced crystallization (SIC) or to the "squeezing" of the crystalline phase in the overall structure, i.e., residual stress effect,[45] since the latter also requires more energy to melt the

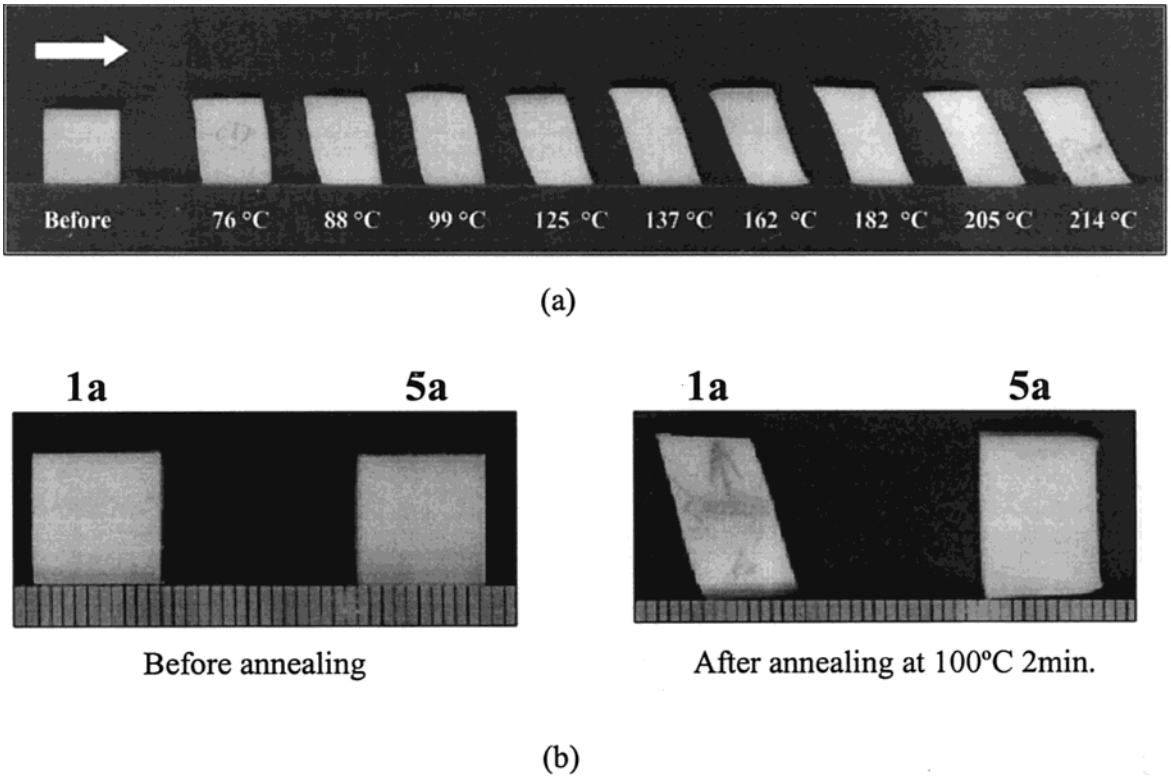

Figure 9. Annealing tests of PET extruded at room temperature and at an extrusion rate of 0.51 mm/s: (a) annealing temperature effect on sample **1a** and (b) comparison of samples **1a** and **5a**. Sample **1a** was cut parallel to LD-FD plane. Sample **5a** was cut perpendicular to FD. The arrow indicates FD.

Table 2. Thermal Characteristics and Density Analyses of PET

sample	DSC melting enthalpy (ΔH, J/g)	density (g/cm^3)
reference PET (before ECAE)	57.642	1.398
sample A1 in region I	64.105	1.388
sample A1 in region III	70.713	1.376
sample A1 anneal at 100 °C for 1 h	53.524	1.385
sample A1 anneal at 100 °C for 2 h	56.161	1.390

crystal. However, the DSC results show that when sample A1 is annealed at 100 °C for 1 and 2 h, the heat of fusion decreases. This result supports the latter speculation; i.e., the residual stress effect is more pronounced. Moreover, the decreases in density (Table 2) and crystallinity determined from wide-angle X-ray scattering (WAXS)[42] further support the residual stress effect on the DSC melting enthalpy data. Meanwhile, Santa Cruz et al.[46] found that the crystallinity and lamellar thickness of PET do not change appreciably when annealed at 120 °C for extended period of time. Therefore, the SIC effect, if any, is considered to be a minor factor in this case.

Discussion

The intent of the present work is to fundamentally understand the lamellar structural evolution of semicrystalline PET during the ECAE process. A combination of SAXS, OM, TEM, and annealing tests was employed.

On the basis of the above findings, it is clear that the ECAE process is effective in shear orienting the lamellar structures in semicrystalline PET. Under the present extrusion condition, the macroscopic deformation angle (θ) of the grid lines is 28°, indicating that the induced shear strain after A1 ECAE is 190%. This value is close to the theoretical value of 200%.[26] ECAE extrusion rate is found to affect the amount of induced shear strain and the maximum temperature rise. This is most likely due to the combined effects between molecular orientation and the thermally activated relaxation of the oriented polymer chains during ECAE.[47,48] Slow extrusion rates give polymer chains more time to relax. Consequently, slow extrusion rates will result in a decreased shear strain and a smaller temperature rise (Figure 4).

During the ECAE process, the original rectangular shape *abcd* will be deformed into parallelogram $a'b'c'd'$ (Figure 1b). During the transformation, the two sides *ab* and *cd* conserve their length and spacing, i.e., $ab = a'b'$ and $cd = c'd'$. The relative displacement between sides $a'b'$ and $c'd'$ along their flow lines builds up the ECAE shear strain (γ) per pass.[35,36] When the material block proceeds through the ECAE die right angular region, the shear strain (γ), which is at an angle of 45° counterclockwise from the FD, will cause the original eqiaxed spherulites to be deformed into nearly ellipsoidal shapes. The long axis of the ellipsoid will be aligned nearly parallel to the maximum tensile direction,[4] i.e., at an angle (α) of nearly 24° counterclockwise away from the flow direction (Figure 10), while the minor axis of the ellipsoid is along the principal compressive strain direction. The OM micrographs shown in Figure 5 further confirm this finding. This result also agrees with the theoretical predictions:[27]

$$\alpha = \frac{1}{2}\arctan\left(\frac{2}{\gamma}\right) \tag{1}$$

$$\gamma = \cot(\theta) \tag{2}$$

Therefore, there is a discrepancy between the macro-

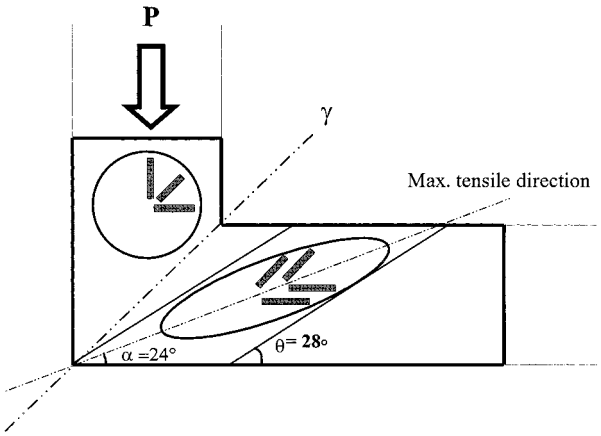

Figure 10. Schematic showing the deformation of spherulites during the A1 ECAE process.

scopic deformation angle (θ), which is measured from the deformed grid lines, and the microscopic deformation angle (α).[30] The angle α decreases with increasing γ, making the difference between macroscopic deformation and microscopic molecular orientation progressively smaller after multiple ECAE passes. Equation 1 is valid only for isotropic material systems. Although the original spherulitical PET is anisotropic at the lamellar scale, the experimental results indicate that the simple shear deformation of semicrystalline PET is nearly homogeneous at the macroscopic (spherulitical) scale. Therefore, the application of eq 1 is adequate in this discussion.[30]

The deformation at the lamellar scale shows that two lamellar orientations are induced after A1 ECAE process. In the fully extruded region (region III), the α-lamellar domain is oriented with the lamellar domain normal tilted at an angle of around 45° clockwise away from FD; while the normal of the β-lamellar domain is almost perpendicular to FD (Figure 6). The reason for this is that since the maximum tensile direction is around 24° counterclockwise away from FD (Figure 10), the lamellae in the polar and the equatorial regions of the spherulite can undergo chain slip more easily than those lamellae in the inclined region. As a result, the lamellae in the inclined region will remain intact,[5,8] which results in the two lamellar orientations observed by SAXS.

The four-point SAXS pattern, i.e., the presence of two lamellar orientations, observed in ECAE has also been found in uniaxial and biaxial rolling of poly(oxymethylene) (POM),[24,25] plane strain compression of high-density polyethylene (HDPE), and PET.[8−10] Many efforts have been made to understand the formation of this structure during the solid-state orientation of semicrystalline polymers.[22,49−51] Peterlin proposed that micronecking is responsible for the evolution of this new morphology.[22] Wilkes explained that the shear gradient across the specimen thickness direction causes the formation of this structure.[50] Recently, Galeski et al.[51] suggested that lamellar thinning, fragmentation, and reconstruction are the most important mechanisms.

The possible evolution of the four-point SAXS pattern is now unambiguously revealed because of the unique ECAE process. The transition scan in sample **1t** (Figure 7) has clearly disclosed the lamellar evolution process during ECAE. The two lamellar orientations in the fully extruded region (III) are actually originated from the same initial lamellar structure in the PET spherulites before the extrusion. Both α- and β-lamellar domains show comparable peak intensity before the billet passes through the shear plane OO′ (scan 10 in Figure 7b). However, as the billet passes through the shear plane, one of the two preferred lamellar orientations, i.e., the β-lamellar domain orientation, becomes weaker with respect to the α-lamellar domain (scans 5 and 9 in Figure 7b). Compared with the orientation of the β-lamellar domain, the orientation of the α-lamellar domain is less affected by the simple shear process since the α-lamellar domain is aligned parallel to the shear plane. It is expected that, after multiple ECAE passes, the α-lamellar domain orientation will be progressively aligned along the flow direction.[36] Contrarily, the β-lamellar domain orientation will become weaker and eventually disappear after multiple ECAE passes. Earlier results on ECAE of LLDPE after four consecutive passes show that, indeed, only one lamellar domain orientation is found to be present and is oriented along the flow direction.[32]

The analysis of the TEM micrograph (Figure 8) shows that, after the ECAE process, the crystalline lamellae are more closely packed to each other. This is due to the interlamellar amorphous material is sheared and compressed after the ECAE process. The compressing of the amorphous phase may easily occur during the early stages of the ECAE process since there is a temperature rise of PET by nearly 50 °C during the extrusion. The temperature rise will bring the material to its rubbery state and reduce the deformation resistance of the amorphous phase. The annealing tests further indicate that after ECAE the molecular chains between the lamellae are well strained. As a result, the initial shape of sample **1a** is partially recovered during the annealing test. An important role of the interlamellar deformation is to help transform the applied strain to the adjacent lamellae and facilitate crystallographic slip.[4]

As mentioned above, the morphological features at different scales of semicrystalline polymers will respond in different manners to accommodate the overall straining. At the micrometer scale, the spherulites will be deformed first. Several models have been proposed in the literature to address this effect.[51−53] The crystalline lamellae in the polar, equatorial, and inclined regions inside the spherulites will experience different modes of deformation.[8] At the molecular chain scale, the molecular chains will be preferentially oriented along the flow direction of the material after large deformation.[24,25] Indeed, the WAXS analysis shows that the *c*-axis of the triclinic PET crystal unit cell is tilted at a small angle with respect to FD in the ECAE-processed samples. This aspect of the research will be addressed in more detail in a subsequent paper.[42]

Most of the models used to explain the formation of the new long period involve the destruction of the preexisting crystalline lamellae and the formation of the new lamellae.[22,51] Crystallographic slip,[8] dislocation propagation,[55−57] and strain- and melting-induced crystallization[58−60] have been identified to be the important mechanisms during this "destruction−reconstruction" process. The present study, however, indicates that, during the large strain simple shear process, the evolution of the new lamellar structure does not necessarily require the reconstruction of the predeformed structures. Although the crystalline phase will generally be destroyed during the deformation, it may

still be possible that some crystalline lamellae are preserved, i.e., through mechanical twinning and the deformation of the amorphous phase.[58] Mechanical twinning might be of particular importance in the deformation of triclinic semicrystalline polymers like PET, which lacks crystal symmetry.[61]

The uniqueness of ECAE is that it will not only provide an unambiguous way to observe microstructural evolution in semicrystalline polymers in the solid state but also improve the physical and mechanical properties of the extrudates. This aspect of results will be reported in a separate paper. Owing to the angular nature of the ECAE die fixture, the gradual evolution of lamellar orientation can be clearly observed. The implementation of ECAE to polymer fabrication still awaits further evaluation. However, it is quite possible that ECAE will become an effective polymer fabrication method and pose a great impact to the field of polymer processing.

Conclusions

By employing the ECAE technique, a high level of shear strain (190%) can be induced in semicrystalline PET after one ECAE pass under the present extrusion conditions. After A1 ECAE process, two lamellar orientations are induced. The surface of one type of lamellae is parallel to the flow direction, while the other at an angle of about 45° counterclockwise away from the flow direction. The analyses of the SAXS patterns from the transition zone sample indicate that the new lamellar orientations are evolved from the original lamellae structure. The annealing test results show that interlamellar shear and interlamellar compression are the dominant deformation mechanisms of the amorphous phase during the A1 ECAE process.

Acknowledgment. The research grants from Dow Chemical and the State of Texas (Grant ARP-98-32191-72380) are greatly appreciated. The authors thank Dr. John D. Barnes at NIST (Gaithersburg, MD) for the discussions on SAXS. The authors also thank Dr. Sittertz-Bhatkar Helga at the Electron Microscopy Center at Texas A&M University for the assistance with the TEM work.

References and Notes

(1) Thomas, L. S.; Cleereman, K. J. *SPE J.* **1972**, *28*, 61.
(2) Southern, J. H.; Porter, R. S. *J. Appl. Polym. Sci.* **1970**, *14*, 2305.
(3) Iwata, T.; Doi, Y. *Macromol. Chem. Phys.* **1999**, *200*, 2429.
(4) Coulon, G.; Castelein, G.; G'Sell, C. *Polymer* **1998**, *40*, 95.
(5) Lin, L.; Argon, A. S. *J. Mater. Sci.* **1994**, *29*, 294.
(6) Keller, A.; Hay, I. L. *J. Mater. Sci.* **1967**, *2*, 538.
(7) Groves, G. W.; Hirsch, P. B. *J. Mater. Sci.* **1969**, *4*, 929.
(8) Bowden, P. B.; Young, R. J. *J. Mater. Sci.* **1974**, *9*, 2034.
(9) Song, H. H.; Argon, A. S.; Cohen, R. E. *Macromolecules* **1990**, *23*, 870.
(10) Bellare, A.; Cohen, R. E.; Argon, A. S. *Polymer* **1993**, *34*, 1393.
(11) Lee, B. J.; Argon, A. S.; Parks, D. M.; Azhi, S.; Bartczak, Z. *Polymer* **1993**, *34*, 3555.
(12) Lee, B. J.; Parks, D. M.; Azhi, S. *J. Mech. Phys. Solids* **1993**, *41*, 1651.
(13) Ahzi, S.; Lee, B. J.; Asaro, R. J. *Mater. Sci. Eng. A* **1994**, *189*, 35.
(14) Yeh, G. S. Y. *Polym. Eng. Sci.* **1976**, *16*, 137.
(15) Jabarin, S. A. *Polym. Eng. Sci.* **1992**, *32*, 134.
(16) Misra, A.; Stein, R. S. *J. Polym. Sci., Polym. Phys. Ed.* **1979**, *17*, 235.
(17) Sun, T.; Pereira, J.; Porter, R. S. *J. Polym. Sci., Polym. Phys. Ed.* **1984**, *22*, 1163.
(18) Göschel, U.; Deutsher, K.; Abetz, V. *Polymer* **1996**, *37*, 1.
(19) Ajji, A.; Guevremont, J.; Cole, K. C.; Dumoulin, M. M. *Polymer* **1996**, *37*, 3707.
(20) Dargent, E.; Grenet, J.; Auvray, X. *J. Therm. Anal.* **1994**, *41*, 1409.
(21) Fu, Y.; Busing, W. R.; Jin, Y.; Affholter, K. A.; Wunderlich, B. *Macromol. Chem. Phys.* **1994**, *195*, 803.
(22) Peterlin, A. *J. Polym. Sci., Part C* **1965**, *9*, 61.
(23) Bartczak, Z.; Cohen, R. E.; Argon, A. S. *Macromolecules* **1992**, *25*, 4692.
(24) Gezovich, D. M.; Geil, P. H. *J. Mater. Sci.* **1971**, *6*, 509.
(25) Gezovich, D. M.; Geil, P. H. *J. Mater. Sci.* **1971**, *6*, 531.
(26) Segal, V. M. *Mater. Sci. Eng. A* **1995**, *197*, 157.
(27) Nadai, A. In *Theory of Flow and Fracture of Solids*; McGraw-Hill: New York,1950; p 147.
(28) Sue, P. L.; Havner, K. S. *J. Mech. Phys. Solids* **1983**, *32*, 417.
(29) Bridgeman, P. W. In *Studies in Large Plastic Flow and Fracture*; McGraw-Hill: New York, 1952.
(30) Bartczak, Z.; Argon, A. S.; Cohen, R. E. *Polymer* **1994**, *35*, 3427.
(31) Aboulfaraj, M.; G'Sell, C.; Ulrich, B.; Dahoun, A. *Polymer* **1995**, *36*, 731.
(32) Sue, H.-J.; Li, C. K. Y. *J. Mater. Sci., Lett.* **1998**, *17*, 853.
(33) Li, C. K. Y.; Xia, Z.-Y.; Sue, H.-J. *Polymer* **2000**, *41*, 6285.
(34) Sue, H.-J.; Dilan, H.; Li, C. K. Y. *Polym. Eng. Sci.* **1999**, *39*, 2505.
(35) Segal, V. M.; Hartwig, K. T.; Goforth, R. E. *Mater. Sci. Eng. A* **1997**, *224*, 107.
(36) Segal, V. M. *Mater. Sci. Eng. A* **1995**, *197*, 157.
(37) Rieker, T. P.; Hubbard, P. F. *Rev. Sci. Instrum.* **1998**, *69*, 3504.
(38) Ruland, W. *Colloid Polym. Sci.* **1978**, *256*, 932.
(39) Samon, J. M.; Schultz, J. M.; Hsiao, B. S. *Polymer* **2000**, *41*, 2169.
(40) Tyagi, D.; McGrath, J. E.; Wilkes, G. L. *Polym. Eng. Sci.* **1986**, *26*, 1371.
(41) Blundell, D. J.; Beckett, D. R.; Willcocks, P. H. *Polymer* **1981**, *22*, 704.
(42) Xia, Z.-Y.; Wang, Z.-G.; Sue, H.-J.; Hsiao, B. S. Manuscript in preparation.
(43) Baltá Calleja, F. J.; Vonk, C. G. *X-ray Scattering of Synthetic Polymers*; Elsevier: Amsterdam, 1989; p 243.
(44) Guan, J. Y.; Wang, L.-H.; Porter, R. S. *J. Polym. Sci., Polym. Phys. Ed.* **1992**, *30*, 687.
(45) Ward, I. M. In *Mechanical Properties of Solid Polymers*; Wiley-Interscience: New York, 1971.
(46) Santa Cruz, C.; Stribeck, N.; Zachmann, H. G.; Baltá Calleja, F. J. *Macromolecules* **1991**, *24*, 5980.
(47) Nobbs, J. N.; Bower, D. I.; Ward, I. M. *Polymer* **1976**, *17*, 25.
(48) Göschel, U. *Polymer* **1996**, *37*, 4049.
(49) Way, J. L.; Atkinson, J. R. *J. Mater. Sci.* **1971**, *6*, 102.
(50) Wilkes, G. L. *J. Mater. Sci.* **1971**, *6*, 1465.
(51) Galeski, A.; Argon, A. S.; Cohen, R. E. *Macromolecules* **1988**, *21*, 2761.
(52) Wang, T. T. *J. Polym. Sci., Polym. Phys. Ed.* **1979**, *12*, 145.
(53) Wilchinsky, Z. W. *Polymer* **1964**, *5*, 271.
(54) Yang, R.; Stein, R. S. *J. Polym. Sci., Part A* **1967**, *25*, 939.
(55) Seguela, R.; Gaucher-Miri, V.; Elkoun, S. *J. Mater. Sci.* **1998**, *33*, 1273.
(56) Predecki, P.; Statton, W. O. *Appl. Polym. Symp.* **1967**, *6*, 165.
(57) Shadrake, L. G.; Guiu, F. *Philos. Mag.* **1976**, *34*, 565.
(58) Asano, T.; Balta Calleja, F. J.; Flores, A.; Tanigaki, M.; Mina, M. F.; Sawatari, C.; Itagaki, H.; Takahasi, H.; Hatta, I. *Polymer* **1999**, *40*, 6475.
(59) Vincent, P. I. *Polymer* **1960**, *1*, 7.
(60) G'Sell, C.; Marquez-Lucero, A.; Gilorminin, P.; Jonas, J. J. *Acta Metall.* **1985**, *33*, 759.
(61) Hertzberg, R. W. In *Deformation and Fracture Mechanics of Engineering Materials*, 2nd ed.; John Wiley & Sons: New York, 1983; Chapter 4.

MA001140W